

# Interfacing Perforated Eardrums with Graphene-Based Membranes for Broadband Hearing Recovery

Chunyan Li, Zhiyuan Xiong, Lei Zhou, Weiluo Huang, Yushi He, Linpeng Li, Haibo Shi, Jiayu Lu,\* Jian Wang, Dan Li,\* and Shankai Yin\*

Eardrum perforation and associated hearing loss is a global health problem. Grafting perforated eardrum with autologous tissues in clinic can restore low-frequency hearing but often leaves poor recovery of high-frequency hearing. In this study, the potential of incorporating a thin multilayered graphene membrane (MGM) into the eardrum for broadband hearing recovery in rats is examined. The MGM shows good biocompatibility and biostability to promote the growth of eardrum cells in a regulated manner with little sign of tissue rejection and inflammatory response. After three weeks of implantation, the MGM is found to be encapsulated by a thin layer of newly grown tissue on both sides without a significant folded overgrowth that is often seen in natural healing. The perforation is well sealed, and broadband hearing recovery (1–32 kHz) is enabled and maintained for at least 2 months. Mechanical simulations show that the high elastic modulus of MGM and thin thickness of the reconstructed eardrum play a critical role in the recovery of high-frequency hearing. This work demonstrates the promise of the use of MGM as a functional graft for perforated eardrum to recover hearing in the broadband frequency region and suggests a new acoustics-related medical application for graphene-related 2D materials.

## 1. Introduction

The eardrum of mammals transfers acoustic signals from sound in air to the vibration of the middle ear ossicles. The eardrum is also a protective barrier that keeps the middle ear free from dirt, debris, and bacteria.<sup>[1]</sup> The vibration of the eardrum in response to sound stimuli is highly frequency dependent. At low frequencies, eardrum vibrates as a whole and in phase with the sound wave for efficient sound transmission.<sup>[2]</sup> However, the vibration of eardrum at high frequencies (e.g.,  $\geq 4$  kHz) becomes fragmented with phase variation across different areas.<sup>[3]</sup> The eardrum structure is complicated in that it features a triple-layered structure with varied density, thickness, and composition across different regions.<sup>[4]</sup> Such a structure is considered to allow mistuned resonances to average out to an overall strong vibration at ossicles for good sound transmission at high frequencies.<sup>[5]</sup>

C. Li, L. Li, H. Shi, S. Yin  
Department of Otorhinolaryngology  
Shanghai Jiao Tong University Affiliated Sixth People's Hospital  
Shanghai 200233, China  
E-mail: yinshankai@china.com

Z. Xiong, D. Li  
Department of Chemical Engineering  
The University of Melbourne  
Melbourne, Victoria 3010, Australia  
E-mail: dan.li1@unimelb.edu.au


L. Zhou  
Department of Otorhinolaryngology-Head and Neck Surgery  
Zhongshan Hospital affiliated to Fudan University  
Shanghai 200032, China

W. Huang  
YouHear Academy  
Guangzhou 510275, China

Y. He  
Shanghai Electrochemical Energy Devices Research Center  
School of Chemistry and Chemical Engineering  
Shanghai Jiao Tong University  
Shanghai 200240, China

J. Lu  
Department of Stomatology  
Shanghai Jiao Tong University Affiliated Sixth People's Hospital  
Shanghai 200233, China  
E-mail: angelinelu@sjtu.edu.cn

J. Wang  
School of Communication Science and Disorders  
Dalhousie University  
Halifax B3J 1Y6, Canada

 The ORCID identification number(s) for the author(s) of this article can be found under <https://doi.org/10.1002/adhm.202201471>

© 2022 The Authors. Advanced Healthcare Materials published by Wiley-VCH GmbH. This is an open access article under the terms of the Creative Commons Attribution-NonCommercial-NoDerivs License, which permits use and distribution in any medium, provided the original work is properly cited, the use is non-commercial and no modifications or adaptations are made.

DOI: 10.1002/adhm.202201471

In addition, the elaborate arrangement of circular and radial fibers in the middle layer provides the eardrum with stiffness critical for high-frequency sound transmission.<sup>[6]</sup> The unique broadband hearing of mammals is crucial for them to adapt to different environments. Sounds with frequencies below 6 kHz for humans provide essential information for speech perception in quiet conditions, while higher-frequency hearing contributes to sound localization and speech perception in noise conditions.<sup>[7]</sup>

Eardrum perforation caused by infection, trauma and tympanic catheterization can reduce both the efficiency and frequency range of sound transmission. If the perforation cannot be self-healed, surgical intervention, such as myringoplasty,<sup>[8]</sup> is needed. In this surgery, the eardrum is grafted with autologous tissues such as temporalis fascia, cartilage, and fat to support the regeneration of the eardrum.<sup>[9]</sup> However, the use of autologous tissue incurs additional incisions, donor site morbidity and especially suboptimal acoustic recovery. The eardrum repaired using myringoplasty is often thickened and leads to a shallowed conical shape and disordered structure of the fibrous layer, which is the layer for the stiffness of the whole eardrum.<sup>[10]</sup> Full restoration of hearing, particularly in the high-frequency region, has yet to be achieved.<sup>[11]</sup> Nonsurgical tissue engineering approaches have also been developed involving the use of various techniques, such as 3D printing or electrospinning of synthetic materials, to make designed artificial scaffolds and to manipulate eardrum regeneration.<sup>[12]</sup> Since most of these biomaterials for sealing the perforation, such as gelatin sponges and silk fibroin, are biodegradable and only temporarily held on the eardrum as a scaffold, the growth of regenerated eardrum tissue is usually not effectively controlled,<sup>[13]</sup> making it challenging to reconstruct the microstructure of the eardrum for a perfect recovery of the mechanical features. In animal studies, a full recovery of hearing could be achieved between 2–4 kHz, as examined by click auditory brainstem response (ABR), but remains challenging in the higher frequency region.<sup>[12c,14]</sup>

The acoustic conduction of the eardrum is determined by its mechanical features in terms of mass and stiffness controlled by the middle fibrous layer.<sup>[4]</sup> Recent experimental and modeling studies show that increasing the stiffness and/or decreasing the mass of the eardrum favors high-frequency sound transmission.<sup>[15]</sup> We thus surmise whether it is possible to graft the perforation with a stiff and lightweight material to modulate the mechanical characteristics of the repaired eardrum for a full recovery of acoustic function. Graphene-based membranes are known to be highly stiff and lightweight.<sup>[16]</sup> Graphene membranes have been successfully used as a vibration component or diaphragm in various acoustic devices, such as microphones and loudspeakers, for excellent acoustic response,<sup>[17]</sup> including the high-fidelity tracking of sound vibration at high frequencies.<sup>[17,18]</sup> The unique acoustic properties of graphene-based membranes inspired us to explore their potential as an alternative functional graft for eardrum repair. To this end, the interactions of graphene-based membranes with the perforated eardrum (i.e., biocompatibility and stability) and the acoustic properties of the resultant “hybrid” eardrum need to be examined.

We have previously prepared multilayer graphene membranes (MGMs) composed of parallelly stacked chemically converted graphene (CCG) nanosheets. They show ultrahigh tangential Young's modulus and can be made very thin.<sup>[19]</sup> In this work, we

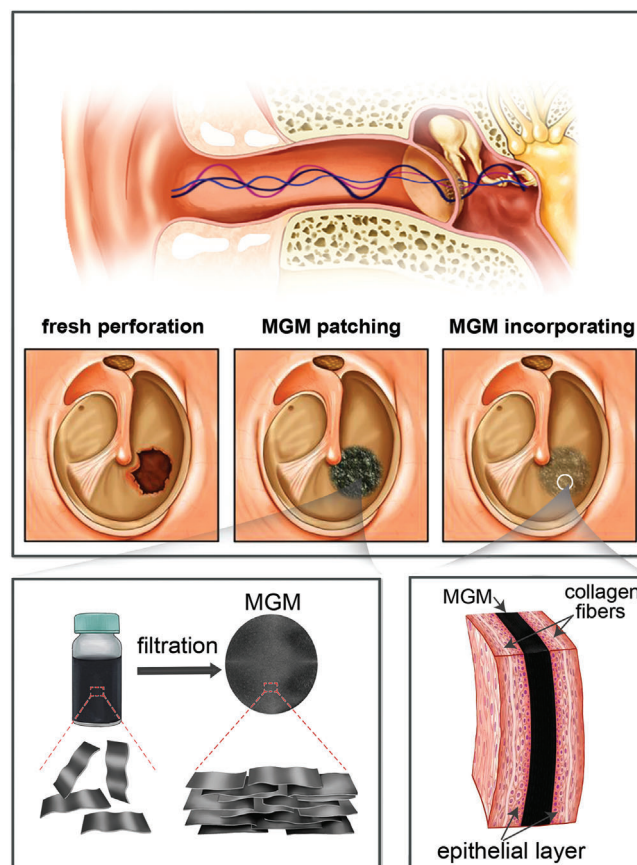


**Figure 1.** Schematic illustration of the MGM incorporation strategy for the acoustic functional recovery of a perforated eardrum. The MGM prepared by parallel stacking of graphene nanosheets is tailored to the size matching the perforation and is patched onto the eardrum. The eardrum tissue grows on both sides to encapsulate the MGM.

explored the use of MGM as a new synthetic graft for eardrum repair (**Figure 1**). We found that covering the perforated eardrum with an MGM that was a few micrometers thick could immediately improve the broadband hearing function of rats. MGMs also appeared to be highly biocompatible to eardrum cells with little tissue rejection and inflammatory response. The MGM is encapsulated by a thin layer of newly grown tissue on both sides. The reconstructed eardrum showed almost the same acoustic function as the natural eardrum.

## 2. Results and Discussion

### 2.1. Preparation and Characterization of MGM

The MGM was prepared by filtering the aqueous dispersion of CCG nanosheets according to our previous method.<sup>[19,20]</sup> The as-prepared membrane had a laminar structure with the CCG nanosheets densely stacked roughly in parallel along the membrane surface (**Figure 2A,B**). By adjusting the volume of the CCG dispersion used in filtration, the thickness of the MGM can be readily controlled in the range between  $\approx 100$  nm and  $\approx 100$   $\mu$ m. The Young's modulus of the MGM with a thickness of 10  $\mu$ m was measured to be  $1.47 \pm 0.16$  GPa and  $19.8 \pm 2.9$  GPa in the normal

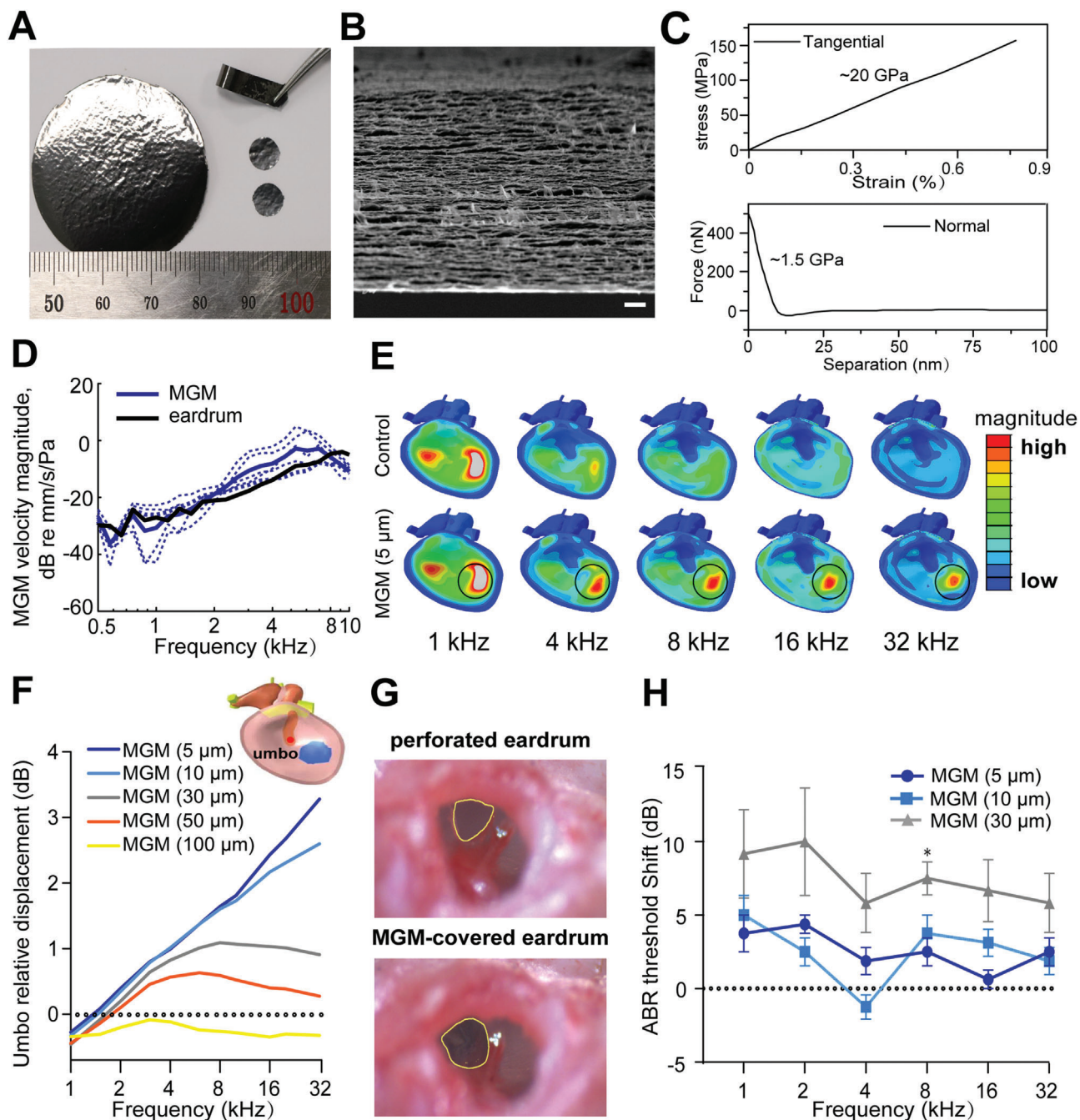


**Figure 2.** Mechanical properties and acoustic function evaluation of the MGM. A) Gross and B) SEM images of the MGM. Scale bar in b: 1  $\mu\text{m}$ . C) Young's modulus of the MGM with a thickness of 10  $\mu\text{m}$  in the normal and tangential directions measured by tensile testing and atomic force microscope (Section S1 in Supporting Information). D) The velocity magnitude measured in the center of the MGM placed on a pars tensa perforation and in the same location of the normal eardrum before perforation. The dotted line represents five different tests, and the solid line represents the mean values of the velocity magnitude for the MGM. E) FEM simulation for steady state vibration pattern of normal eardrum (upper row) and eardrum patched with MGM (down row) under 90 dB SPL sound stimulation at frequencies ranging from 1 to 32 kHz. The color bar indicates the vibration amplitude. The black circle indicates the area of MGM patching. F) The relative displacement of the umbo as a function of frequency calculated by FEM. The displacement of the normal eardrum (baseline) served as the reference (0 dB). G) Images of the eardrum before and after MGM patching. H) ABR threshold shifts recorded immediately after the perforation was patched by MGM of different thicknesses. Error bars represent the s.e.m.; \*  $p < 0.05$ .



and tangential directions, respectively (Figure 2C and Figure S1, Supporting Information). Moreover, the MGM showed a tangential mechanical strength of  $\approx 150$  MPa (Figure 2C), which was the highest value among the membrane-like eardrum patches made of other biomaterials, such as silk,<sup>[21]</sup> chitosan,<sup>[22]</sup> and cartilage.<sup>[23]</sup> As shown in Figure 2A, the MGM was freestanding and flexible and could be readily tailored into small, rounded pieces, which could then be manipulated by tweezers for subsequent patching operations. The MGM could readily adhere to the eardrum along the edge of the perforation after the membrane was simply placed on site (Video S1, Supporting Information).

We first characterized the vibrating behavior of the MGM by a laser Doppler vibrometer (LDV). For the vibrating measurement, MGM (5  $\mu\text{m}$ ) was placed on a pars tensa perforation with no edge fixation to simulate the application in a physiological environment. The vibrating velocity at the center of the MGM in response to sound stimulation with a 90 dB sound pressure level (SPL) in the frequency range of 0.5–10 kHz is shown in Figure 2D ( $n = 5$ ) and compared with that at the same location of the normal eardrum before perforation ( $n = 5$ ). It was found that both groups showed similar frequency response curves, with the first vibrating peak located at  $\approx 0.75$  kHz. Additionally, finite element modeling (FEM) was used to simulate the vibrating patterns of the normal eardrum and MGM-patched eardrum. The simulation was performed by substituting  $\approx 50\%$  of the anterior half of pars tensa with a 5  $\mu\text{m}$  thick MGM (Figure 2E, black circle area). The vibrating patterns of the MGM-patched eardrum were similar to those of the normal eardrum. However, the vibrating amplitude within the region of the MGM was even larger than that of the normal control at frequencies  $> 4$  kHz (Figure 2E, Video S2, Supporting Information). These studies clearly showed that the MGM patch can serve as a vibrating diaphragm for sound transmission.

## 2.2. Immediate Hearing Recovery after Interfacing the Perforated Eardrum with MGM

We investigated how the freshly patched MGM changed the sound transmission of the eardrum through both mechanical modeling and the test of hearing in animal experiments. We used FEM to simulate the displacement of an eardrum in which a perforation taking  $\approx 50\%$  of the anterior half of pars tensa (see the inset in Figure 2F) was covered by MGM with different thicknesses.<sup>[15,24]</sup> As shown in Figure 2F, the umbo vibration of the patched eardrum relative to that with normal eardrum gradually increased as the thickness of the MGM decreased from 100  $\mu\text{m}$  (e.g., -0.35 dB at 16 kHz) to 5  $\mu\text{m}$  (e.g., 2.43 dB at 16 kHz). The modeling results indicated that a thinner MGM was more efficient for the recovery of hearing function.

We further evaluated the hearing function recovery of rats after the perforation was freshly patched (Figure 2G) with ultrathin MGM (5–30  $\mu\text{m}$ ) by measuring the threshold with tone burst ABR. As shown in Figure 2H, patching with a thinner MGM resulted in a smaller ABR threshold shift. In the two groups in which the perforation was covered with 5- and 10  $\mu\text{m}$  thick MGM, the ABR threshold shifts were less than 5 dB compared to the values before perforation. A significant group (thickness) effect was found ( $F_{(2, 19)} = 9.564$ ,  $p = 0.0013$ ) in a two-way ANOVA against

the factors of group and frequency. However, the cross-group difference was only significant at 8 kHz, which was demonstrated by a post hoc test (Tukey's method,  $q = 4.830$ ,  $p = 0.015$ ) between the 30  $\mu\text{m}$  ( $n = 6$ ) and 5  $\mu\text{m}$  groups ( $n = 8$ ). These results showed that thinning the MGM to a few micrometers could greatly recover the hearing functions of the perforated eardrum.

We used a graphene hydrogel membrane (MGHM) as a reference patch to study the role of the mechanical properties of MGM in its ability to recover hearing. Similar to the fabrication of the MGM, the MGHM was prepared by filtering an aqueous CCG dispersion, while  $\approx 90$  wt% water remained inside the MGHM.<sup>[25]</sup> Therefore, the MGHM shares a similar chemical composition with the MGM but has a significantly lower Young's modulus ( $\approx 1.5$  MPa in the normal direction and  $\approx 70$  MPa in the tangential direction, Figure S2, Supporting Information) than the MGM. When the perforation was patched with the MGHM (10  $\mu\text{m}$  thick), the ABR threshold shifts were found to be significantly greater than those of the stiffer MGM of the same thickness at the high frequencies tested (16 kHz and 32 kHz, Figure S2, Supporting Information). This result suggested that the high elastic modulus of the MGM was crucial for its superior hearing recovery performance.

## 2.3. Biocompatibility of MGM In Vitro

Critical criteria for synthetic grafts incorporated into eardrum include interface compatibility and interface properties for cell proliferation and adhesion, which are crucial factors for promoting the healing process. The material interface should interact and allow dynamic reciprocity in initiating and perpetuating tissue development.<sup>[13b]</sup> To investigate the capability of MGM as an implantable eardrum graft, the interaction between MGM and eardrum was studied both in vitro and in vivo. For the in vitro study, living eardrum cells (fibroblasts and epithelial cells, Figure S3, Supporting Information) were labeled by the polyanionic dye calcein with green fluorescence and were contrasted with the dead cells that were labeled by EthD-III with red fluorescence.<sup>[26]</sup> A small number of dead fibroblasts (Figure 3A) and epithelial cells (Figure S4, Supporting Information) were observed on both the glass and MGM surfaces. These results indicated that the MGM was nontoxic for eardrum cells. Subsequently, the cell proliferation, morphology and adhesion on the MGM were investigated. The percentage of Ki-67-positive fibroblasts was higher on the MGM surface than on glass 24 h after seeding ( $86.3 \pm 3.1\%$  vs  $70.8 \pm 2.7\%$ , t-test,  $t = -11.757$ ,  $p < 0.0001$ , Figure 3B,C). Good proliferation of epithelial cells was also observed in the culture on both surfaces, but there was no significant difference between the two (MGM:  $86.3 \pm 7.9\%$  and glass:  $84.4 \pm 7.7\%$ , t test,  $t = -0.541$ ,  $p > 0.05$ ; Figure S4, Supporting Information). Scanning electron microscope (SEM) imaging showed that fibroblasts (Figure 3D) and epithelial cells (Figure S5, Supporting Information) were tightly attached to the MGM surface on Day 1 after seeding. At Day 3, the cells were found to be well spread over the MGM as a flat layer. Compared to the cells on glass, fibroblasts on the MGM had more cellular microextensions, as shown by actin staining. A higher-than-glass adhesion between the MGM and the cells was demonstrated by a larger number of focal adhesion sites along the edge of protrusions of fibroblasts (stained by vinculin foci)

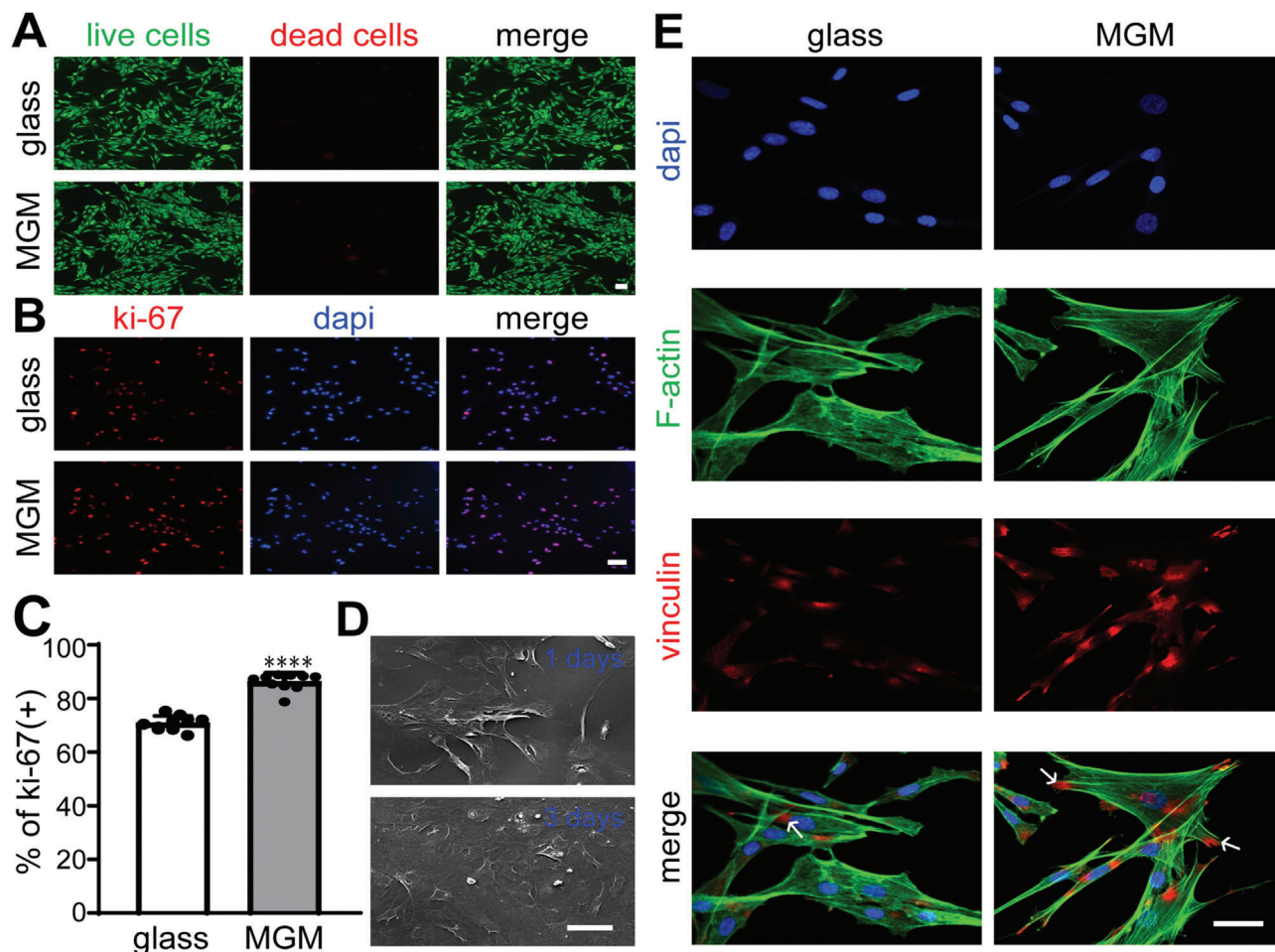


**Figure 3.** Evaluation of the interaction between MGM and eardrum cells. A) Live-dead staining 24 h after cell seeding on glass (upper row) and MGM (bottom row). Scale bar, 200  $\mu$ m. B) Immunofluorescence staining of Ki-67 (red) and counterstaining with DAPI (blue) were performed on fibroblasts 24 h after cell seeding on glass (upper row) and MGM (bottom row). Scale bar, 200  $\mu$ m. C) The evaluation of Ki-67-positive cells was recorded as the percentage of labeled cells. Values of % Ki-67 were obtained by randomly enumerating positive cells from 10 fields at a magnification of 200 times. D) SEM micrographs of fibroblasts 1 and 3 d after seeding on the MGM. Scale bar: 50  $\mu$ m. E) Fluorescence images of the actin cytoskeleton (green) and vinculin (red) and merged pictures of fibroblasts obtained from confocal microscopy (20 $\times$  objective) 12 h after cell seeding on glass (left) and MGM (right). Scale bar, 50  $\mu$ m. White arrows indicate the location of vinculin foci. Error bars represent the s.e.m.; \*\*\*\*:  $p < 0.0001$ .

(Figure 3E).<sup>[27]</sup> A similar result was found for the adhesion of epithelial cells (Figure S5, Supporting Information). These results indicated that MGM had a biocompatible and bioactive interface for eardrum cell growth, proliferation, and adhesion.

#### 2.4. MGM-Incorporated Eardrum Construction and Biocompatibility of MGM In Vivo

In the in vivo study, morphological observation was performed three weeks after MGM implantation.<sup>[24b]</sup> We found that the surface of the MGM was fully covered by newly grown eardrum tissue composed of thin and ordered epithelial cell layer and a smooth collagen fiber layer along both sides of the MGM (Figure 4A). This is very different from the regenerated eardrum by the scaffold tissue engineering technique in previous reports, which often has only one layer of collagen fiber.<sup>[12a,24b]</sup> Surprisingly, no obvious cellular indicators of rejecting response

and inflammatory response were observed around the MGM in the reconstructed eardrum (Figure 4A). In striking contrast, significant epithelial hyperplasia accompanied by edema, red blood cell extravasation, and karyorrhexis was found in the self-healed eardrum, suggesting a serious excessive repairing response. The proliferative collagen fiber layer in the self-healed eardrum was thickened, disorganized, or absent (the right column in Figure 4A, Figure S6, Supporting Information). The MGM patched area of the eardrum was thicker than the corresponding area in normal eardrum but much thinner than that in self-healed eardrum ( $56.8 \pm 30.0$   $\mu$ m,  $12.5 \pm 1.5$   $\mu$ m, and  $156.2 \pm 53.4$   $\mu$ m, respectively, for the MGM, normal and self-healing groups). A significant overall difference across the groups was demonstrated by a one-way ANOVA ( $n = 4$  in each group,  $F(2, 9) = 17.36$ ,  $p = 0.0008$ ). Post hoc tests (Tukey's method) showed a significant difference between the MGM and self-healing groups ( $q = 5.678$ ,  $p = 0.0077$ ). However, the difference between the MGM and normal groups was not significant ( $q = 2.444$ ,

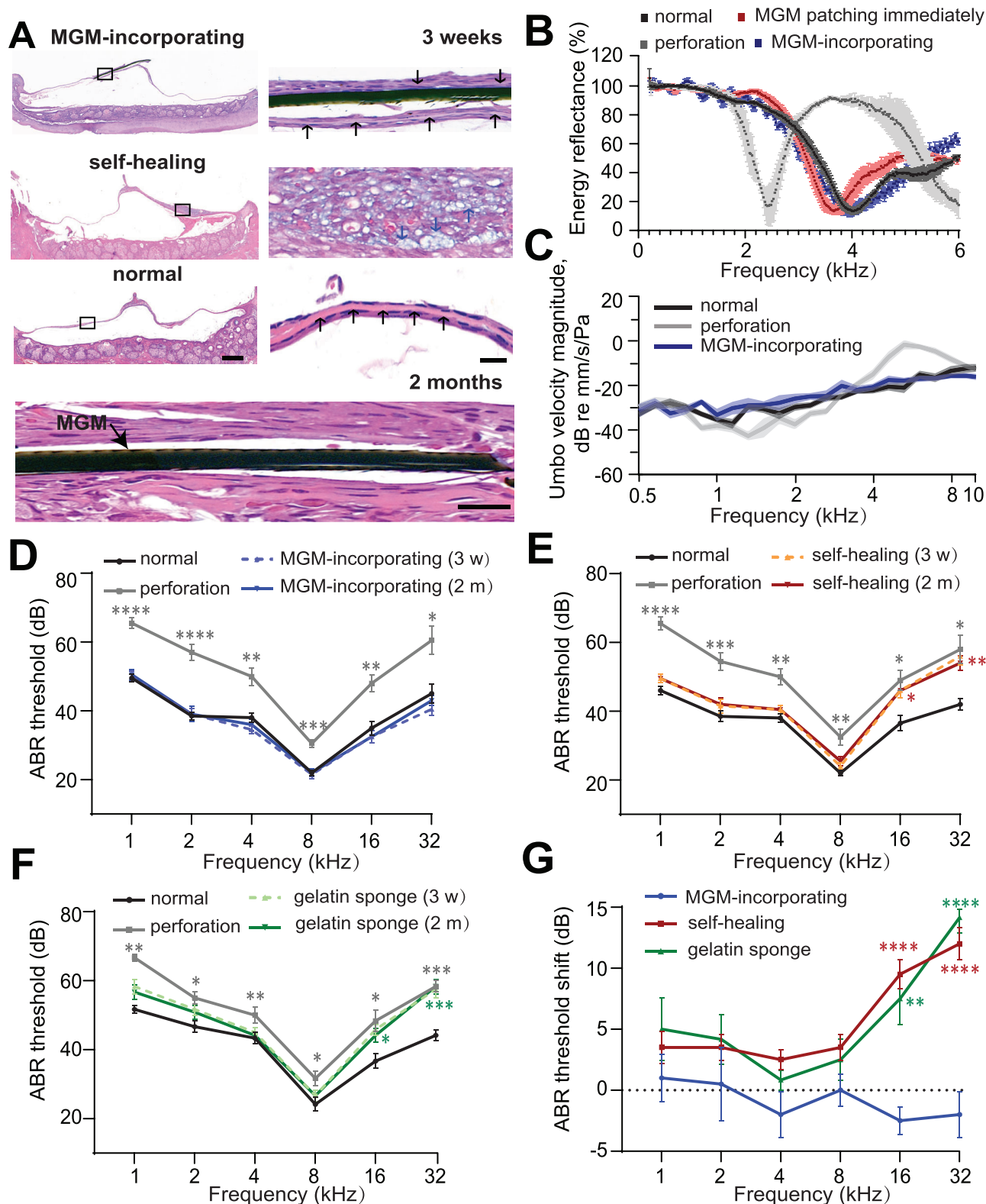


**Figure 4.** Histological and functional evaluation of the MGM-incorporated eardrum. A) H&E staining observation of MGM-incorporated eardrum (three weeks postoperatively), self-healed eardrum (three weeks postoperatively), and normal eardrum. Scale bar, 200  $\mu$ m. Enlarged photomicrographs of H&E staining of the area indicated by the black frame are shown on the right. The collagen fibers are indicated by black arrows. The blue arrows indicate tissue edema. Scale bar, 10  $\mu$ m. Bottom: H&E staining of the MGM-incorporated eardrum 2 months postoperatively. Scale bar, 10  $\mu$ m. B) Energy reflectance measured preperforation (normal, black), postperforation (gray), immediately after MGM patching (5  $\mu$ m) (red) and MGM patching for three weeks



$p = 0.25$ ). These results demonstrated that MGM guided the growth of thin and organized eardrum tissues on its two sides to seal the perforation. The superior performance of MGM may be related to its bioactive interface properties for regulating inflammation and immunity in regenerated tissue.<sup>[28]</sup>

We further evaluated the long-term biostability and biocompatibility of MGM patching. As shown in Figure 4A (bottom), after implantation for 2 months, the structure and thickness of the MGM were retained without obvious changes. We did not observe signs of biodegradation of MGM, such as surface cracking, during the observation period.<sup>[29]</sup> The eardrum cells grew well around the MGM without obvious morphological differences from the normal eardrum control. HE staining also showed no complications, such as epithelial hyperplasia, granuloma, or supuration, in the MGM-incorporated eardrum.

## 2.5. Acoustic Function of the MGM-Incorporated Eardrum

Furthermore, middle ear function was investigated in rats with MGM-reconstructed eardrum. The eardrum needs to transfer acoustic energy into motions of the malleus for effective sound transmission. The energy transmission of the middle ear with MGM-incorporated eardrum was measured by wideband acoustic immittance (WAI) (Figure S7, Supporting Information).<sup>[30]</sup> The WAI test was performed before perforation (the control), immediately after perforation, and three weeks after the patching of the perforation by the MGM ( $n = 4$ ). In the normal ears, the energy reflectance-frequency curve was sharply notched at approximately 4 kHz (Figure 4B). The perforated eardrum showed the strongest energy reflectance up to 90% at approximately 4 kHz. Immediately after MGM patching, the reflectance curves recovered close to the control. The notched frequency in the reflectance-frequency curve was slightly lower than that in the normal eardrum. After MGM patching for three weeks, the reflectance curves highly overlapped with those of the normal controls (Figure 4B), with a small difference above 5 kHz. A similar recovery was also observed in the impedance magnitude curve (Figure S8, Supporting Information). These results demonstrated that middle ear function was well repaired by incorporating MGM into the perforated eardrum.

The vibration behavior of the MGM-incorporated eardrum was tested by LDV (Figure S7, Supporting Information). Similar to previous studies,<sup>[31]</sup> the umbo velocity amplitude exhibited a prominent reduction within the range of 0.5–4 kHz but a slight increase within the range of 4–10 kHz after eardrum perforation. The curves of umbo velocity amplitude highly overlapped with those of the normal controls ( $n = 13$ ) three weeks after MGM patching ( $n = 7$ ) (Figure 4C). Although the frequency is limited up to 10 kHz in the LDV test by the technology, these measurements provided evidence of how the incorporation of the MGM recovered the vibration response of the perforated eardrum.

We subsequently evaluated the recovery of hearing function of rats with MGM-incorporated eardrum through the ABR test. The ABR thresholds were found to be largely recovered between 1 and 8 kHz three weeks after perforation in both groups in which the eardrum was self-healed or repaired by MGM with a 5  $\mu\text{m}$  thickness. The key advantage of the MGM incorporation was the full recovery of the ABR threshold to the normal level at all kHz frequencies (Figure 4D), whereby the threshold shift remained obvious in the self-healing group at frequencies above 16 kHz (Figure 4E) at three weeks postperforation. The hearing recovery results of the MGM-incorporating group were persistent during the observation period of 2 months postperforation (Figure 4D). Similar to the self-healing group, we also found that patching treatment using the biodegradable gelatin sponge could not recover the hearing deficiency of perforated eardrum at frequencies  $\geq 16$  kHz (Figure 4F). We verified the difference between the groups in a two-way ANOVA against grouping and frequency with a significant group effect in the ABR threshold shifts between the self-healing group ( $n = 10$ ), gelatin sponge group ( $n = 6$ ) and the MGM-incorporating group ( $n = 10$ ) ( $F_{(2, 23)} = 18.62$ ,  $P < 0.0001$ ). Post hoc analysis (Tukey method) showed that the differences among the three groups were significant at 16 kHz (MGM-incorporating group vs self-healing group:  $q = 10.50$ ,  $p < 0.0001$ ; MGM-incorporating group vs gelatin sponge group:  $q = 5.855$ ,  $p < 0.01$ ) and 32 kHz (MGM-incorporating group vs self-healing group:  $q = 8.664$ ,  $p < 0.0001$ ; MGM-incorporating group vs gelatin sponge group:  $q = 9.489$ ,  $p < 0.0001$ ) (Figure 4G), favoring the MGM group with the smallest threshold shifts. These results demonstrated that incorporation of the MGM patch enabled complete and long-term stable recovery of broadband frequency auditory function of the rats with perforated eardrum, particularly in high-frequency.

## 2.6. The Mechanism of the Acoustic Function Recovery of MGM-Incorporated Eardrum

We further used FEM to shed light on the mechanism of broadband hearing sound transmission in the MGM-incorporated eardrum. As shown in Figure 5A, this modeling simulated a fully repaired eardrum, in which the MGM was set to be the middle layer and covered by epithelial layers on its two sides in the repaired area (Figure 5A). First, the natural frequency of the eardrum was highly sensitive to the tangential modulus change in the middle layer (Figure 5B): the natural frequency of the MGM-repaired eardrum relative to the normal eardrum (called the natural frequency shift) increased with increasing Young's modulus of the MGM. The natural frequency of the MGM patched eardrum was higher than that of normal eardrum at all selected modes when the MGM modulus was higher than 2 GPa. Second, we examined how the thickness of the epithelial layer along the two sides of the MGM impacted the natural frequency. The results showed that increasing the thickness of the

(blue, MGM-incorporating). Dashed lines represent the standard error ( $n = 4$ ). C) The umbo velocity magnitude measured in normal (black) ( $n = 13$ ), perforated (gray) ( $n = 13$ ) and MGM-incorporated eardrums (5  $\mu\text{m}$ ) (blue) ( $n = 7$ ). Shading around the line represents the standard error. D–F) ABR threshold measured preperforation (normal, black), postperforation (gray), three weeks and two months after MGM patching ( $n = 10$ ), self-healing ( $n = 10$ ) and gelatin sponge patching ( $n = 6$ ). G) Comparison of the threshold shifts among the self-healing group, gelatin sponge group and the MGM-incorporating group. Error bars represent the s.e.m.; \*,  $p < 0.05$ ; \*\*,  $p < 0.01$ ; \*\*\*,  $p < 0.001$ ; \*\*\*\*,  $p < 0.0001$ .

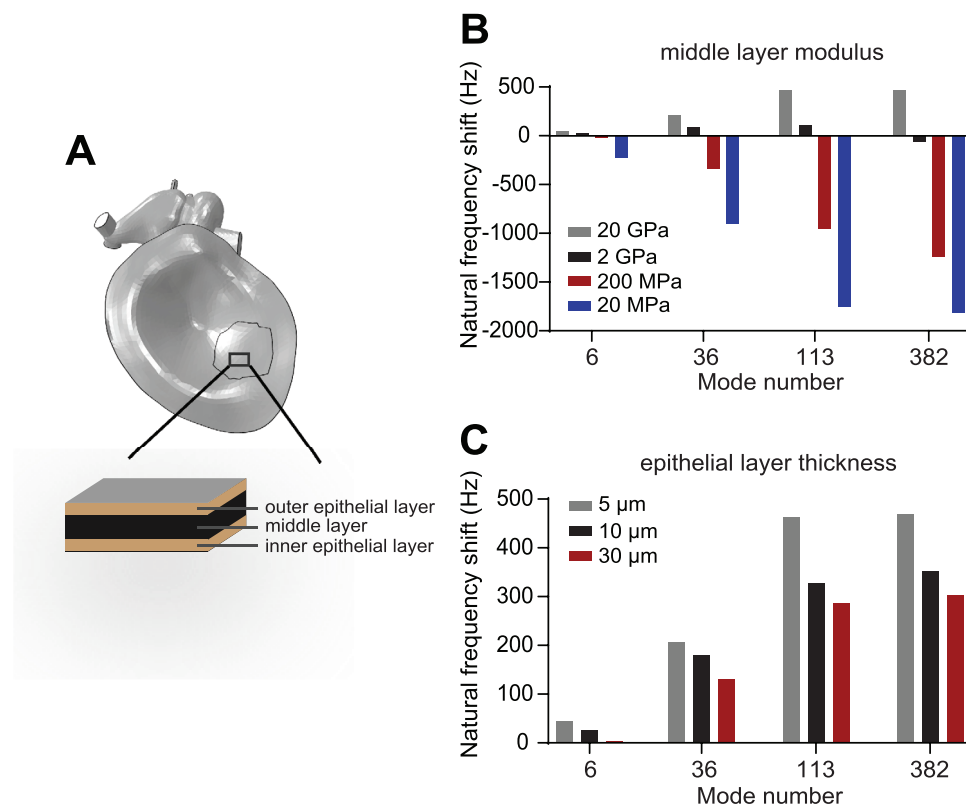


**Figure 5.** Analysis of the natural frequency of vibration of MGM-incorporated eardrum by FEM. A) The schematic diagram of the FEM design. B) The effect of the middle layer (MGM) modulus on the natural frequency shift of the MGM-incorporated eardrum relative to the normal eardrum. The thicknesses of the MGM and epithelial layers are set to 5  $\mu\text{m}$  and 10  $\mu\text{m}$ , respectively. C) The effect of epithelial layer thickness on the natural frequency shift of the MGM-incorporated eardrum relative to the normal eardrum. The thickness of the MGM is set to 5  $\mu\text{m}$ , and the modulus of the MGM is set to 20 GPa.

epithelial layers (from 5 to 30  $\mu\text{m}$  on each side of the MGM) decreased the natural frequency shift of the MGM reconstructed eardrum (Figure 5C). The epithelial layer of the MGM-patched eardrum was much thinner than that of the self-healed eardrum. Therefore, the thinner epithelial layer in MGM patched eardrum likely favors an increase in the natural frequency of the regenerated eardrum. In summary, our FEM results showed that the high modulus of MGM and the low thickness of the tissue layer benefited the recovery of high-frequency hearing of the regenerated eardrum by increasing the natural frequency.

This result is supported by the numerical calculation of the biomechanical properties of the regenerated eardrum (see details in Supporting Information). Due to the extremely high tangential modulus of the MGM ( $19.8 \pm 2.9$  GPa), the tangential modulus of the MGM-incorporated eardrum is calculated to be  $\approx 3.4 \pm 1.8$  GPa, which is much higher than that of the normal eardrum or the self-healed eardrum whose tangential modulus is in the range of approximately tens of MPa. This high tangential modulus is reported to benefit the high-frequency vibration of the eardrum.<sup>[15]</sup> However, as also pointed out in previous studies,<sup>[15]</sup> increasing the modulus of the eardrum will adversely attenuate its vibration amplitude at low frequencies. In our case, due to the thin thickness of the MGM and cell layers that cover it, the bending stiffness of the MGM-incorporated eardrum ( $2.3 \times 10^{-7}$  N m) is much lower than the value of the self-healed eardrum ( $3.2 \times$

$10^{-6}$  N m). Although this bending stiffness is higher than the value of the normal eardrum ( $6.5 \times 10^{-9}$  N m), it makes the MGM-incorporated eardrum sufficiently flexible to vibrate under a low-frequency sound stimulus. Therefore, the low-frequency sound transmission of the MGM-incorporated eardrum is simultaneously recovered with the high-frequency sound transmission.

### 3. Conclusion

In conclusion, we have examined the potential of interfacing perforated eardrum with MGM to recover broadband sound transmission function of eardrum. The MGM showed good biocompatibility for promoting eardrum cell proliferation and adhesion. When used as an eardrum graft, the MGM guided thin and regular eardrum tissue regeneration on its two sides to seal the perforation without significant signs of tissue rejection and inflammatory response. Due to its high elastic modulus and low thickness, the natural frequency of the MGM reconstructed eardrum is increased to benefit high-frequency sound transmission.

Our strategy is different from traditional myringoplasty and previous scaffolding-based bioengineering for eardrum repair, in which the grafts are adsorbed, degraded, or detached during the closure of perforation. Instead, the MGM grafts are stably kept inside the regenerated eardrum, enabling the use of the unique sound transmission properties of graphene to bring unprece-



dented hearing recovery performance at both low and high frequencies. Many eardrum repair studies focus on reconstructing the complex eardrum architecture for hearing recovery. Our work suggests an alternative way to optimize the acoustic functional recovery of perforated eardrum by designing synthetic grafts with specific mechanical properties. Further work is being planned to examine the performance of MGM-incorporated eardrum repair in different eardrum injury models for future clinical applications.

## 4. Experimental Section

**Preparation of MGM:** CCG nanosheets were prepared by chemical reduction of an aqueous graphene oxide dispersion acquired by chemical oxidation and exfoliation of raw graphite using the previous method.<sup>[32]</sup> MGM was fabricated by filtering a certain volume of CCG dispersion ( $0.5 \text{ mg mL}^{-1}$ ) through a porous polycarbonate membrane with a 100 nm pore size (Isopore membrane from Millipore Co., USA). During this process, the CCG nanosheets gradually deposited on the filter membrane to form a continuous membrane. If the vacuum pump was stopped when there was no water left on the deposited membrane, a wet MGHM with 90 wt% was obtained. If the vacuum pump was stopped until all the water was pumped out, a dry MGM could be obtained. In this work, dry MGM was mainly used as a model of stiff and flexible membranes and chose MGHM as a reference. The as-prepared MGM was carefully peeled off from the filter membrane and punched into circular pieces with the desired area. They were further sterilized by autoclaving prior to use.

**FEM Construction and Validation:** The FEM used in this study was constructed based on the previous publications.<sup>[24a,33]</sup> The pars tensa of the eardrum in the present model was divided into three layers: the outer epithelial layer, the middle layer and the inner epithelial layer. The outer and inner epithelial layers were assumed to be isotropic, while the middle layer was assumed to be orthotropic in radial and circumferential directions.<sup>[34]</sup> The thicknesses of the outer layer, middle layer, and inner layer of the pars tensa were set to 0.005, 0.05, and 0.005 mm, respectively. The Young's modulus of the outer and inner layers of the eardrum was  $1.0 \times 10^7 \text{ Pa}$ . The Young's modulus of the middle layer was  $2.0 \times 10^7 \text{ Pa}$  in the circumferential direction and  $3.2 \times 10^7 \text{ Pa}$  in the radial direction.<sup>[10b]</sup> The materials of both the inner and outer layers of the eardrum were assumed to be viscoelastic with the same parameters as the published study.<sup>[33]</sup> The Young's modulus of the tympanic annular ligament of the model was modified based on cross calibration and was set to  $3.0 \times 10^6 \text{ Pa}$ . The density of the soft tissues was set to be  $1.0 \times 10^3 \text{ kg m}^{-3}$ , and the Poisson ratio was set to be 0.3 for all middle ear components. The Rayleigh damping parameters were set as  $\alpha = 0$  and  $\beta = 7.5 \times 10^{-5} \text{ s}$  for all solid components. The external ear canal and middle ear cavity were not included in the FEM.

The FEM model was validated by comparing the calculation results with previous studies (see the validation process in Figure S9, Supporting Information). After validation, 90 dB SPL was loaded on the outside of the eardrum, and steady-state dynamic analysis was conducted over a frequency range from 1 to 32 kHz in Abaqus (v6.10-1, Simulia, Inc., Providence, USA). The perforation area was set to  $7.2 \text{ mm}^2$ . The displacement of the umbo was extracted and plotted. The Lanczos method was used to calculate the natural frequency of the simulated models.

**Animal Experiments:** All study protocols complied with the guiding principles for the care and use of animals and were approved by the Animal Welfare Ethics Committee of Shanghai Sixth People's Hospital (Approval number 2020-0265). Newborn Sprague–Dawley (SD) rats (postnatal days 1–2) were used for harvesting eardrum cells for immunofluorescence staining and electron microscopy observation. Adult male SD rats (8–10 weeks) were used for the animal model study. All animals were anesthetized with sodium pentobarbital ( $55 \text{ mg kg}^{-1}$ , intraperitoneal).

**Eardrum Cell Culture:** After animal anesthetization, the external ears were removed, and the tympanic bullas were isolated. Eardrums were peeled off the tympanic ring using forceps. The harvested eardrums were rinsed in phosphate-buffered saline (PBS) (Gibco, USA). Small pieces of

eardrum tissue were placed in six-well culture plates (BD Biosciences, Australia) and covered with coverslips. The derived cells were incubated in a humidified cell culture incubator at  $37^\circ\text{C}$  with 5% carbon dioxide ( $\text{CO}_2$ ). For fibroblasts, eardrum tissue was cultured in Dulbecco's modified Eagle's medium (DMEM) (Invitrogen, USA) containing 10% FBS. Epithelial cells were cultured in keratinocyte serum-free medium (KFSM, Thermo, USA). Penicillin G sodium ( $100 \text{ U mL}^{-1}$ ) and streptomycin sulfate ( $100 \text{ mg mL}^{-1}$ ) were added to both media. The culture medium was replaced every 2 d.

**Immunofluorescence Staining of Eardrum Cells:** The eardrum cells were seeded on the MGM for 24 h. A Live/Dead Staining Kit (ScienCell, USA) was used to evaluate the potential cytotoxicity of the MGM. Cells were incubated in 1 mL of PBS in a culture dish, followed by the addition of  $2 \mu\text{L}$  of staining solution. Cells were observed immediately under a fluorescence microscope (Ts2R; Nikon, Japan).

Conventional immunofluorescence was used to identify cell types, label proliferating cells and evaluate adhesion characteristics. Briefly, cells were cultured on coverslips or MGM in culture dishes. The cells were rinsed with PBS and then fixed in 4% PFA for 20 min. The PFA was removed, and the cells were rinsed at least three times with 0.3% PBS-X. Then, the cells were treated with 0.1% Triton X-100 for 20 min to permeabilize the cells. The process was blocked by rinsing three times with PBS and treatment with 1% bovine serum albumin (BSA) (Sigma, USA) for 20 min at  $37^\circ\text{C}$ . The primary antibody was diluted in PBS and then applied to the slices overnight at  $4^\circ\text{C}$ . The cells were washed five times with PBS and incubated with secondary antibodies for 1 hour at room temperature in a dark environment. The coverslips or MGM were then mounted onto glass slides using DAPI-Fluoromount (Sigma, USA). The cells were visualized with a fluorescence microscope (Ts2R; Nikon, Japan) or confocal microscope (LSM 710, ZEISS, Germany). The primary antibodies used in this study were anti-pan cytokeratin (Abcam, UK), anti-vimentin (Proteintech, USA), anti-Ki-67 (Abcam, UK), anti-vinculin (Sigma, USA) and phalloidin-iFluor (Abcam, UK).

**Animal Models and Histological Evaluation:** All animals were examined to exclude middle ear pathology using otomicroscopy before the experiments. The perforation was mechanically created using a micropick under a surgical microscope on the anterior half of the pars tensa of the eardrum ( $\approx 1.5 \text{ mm}$  in diameter measured by a periodontal probe) on both sides of the ears. MGM (trimmed into pieces  $\approx 1.8 \text{ mm}$  in diameter) was steam sterilized and placed onto the perforated eardrum on the right side of the ear using the transcanal overlay technique. The other side was left for spontaneous healing as a control. As shown in Video S1 (Supporting Information), after the fresh perforation was made, MGM was delivered into the ear canal with a periodontal probe and then pushed gently to cover the perforation. The modeling results showed that the small bending deformation of the MGM had little influence on the vibrating response of the patched eardrum (Figure S10, Supporting Information). The implantation operation needs to be carefully controlled to avoid damage to the thin MGM or the eardrum. In another animal group, sterile gelatin sponges were placed onto the fresh perforation using tweezers. The eardrums were observed every week to determine the position of the MGM or gelatin sponges under a surgical microscope (M320, Leica, Germany). If the materials were displaced from the hole, the animals were excluded. All animals survived and showed no postoperative complications after surgery. For morphological evaluation, the eardrums with the bony annulus were extracted from the tympanic bulla and fixed in 10% neutral buffered formalin for 24 h. The samples were then decalcified in 10% hydrochloric acid formaldehyde decalcification solution for 3 d. After paraffin embedding, a total of  $3 \mu\text{m}$  sections were cut and stained with hematoxylin and eosin (H&E). The stained sections were digitally scanned using a Panoramic MIDI scanner (3D HISTECH, Hungary). The thickness of the regenerated eardrum was averaged from 3 representative points in the perforated area.

**WAI Measurement:** The HearID system (Mimosa Acoustics, Inc., Champaign, Illinois) was used for the measurement of wideband energy reflectance and impedance magnitude. This system consists of a laptop with the installation of HearID 5.1 software, an ER-10C probe (Etymotic Research, Illinois) with a probe-adaptor cable, and a calibration cavity set of four cavities. The probe was calibrated daily with HearID before the

start of every experiment by using the Mimosa Acoustics Calibration Cavity Set. Prior to starting the test, an in-the-ear calibration using a 1 kHz tone was made to establish the overall level for outputting the chirp and tonal stimuli. The wideband chirp stimulus was output repeatedly at 60 dB SPL for 4 to 6.4 s and analyzed within a 0.2–6 kHz frequency range. After finishing the sweeps, the software represented the wave curves of energy reflectance and impedance magnitude. Data were collected using the program in HearID.

**LDV Measurement:** A speaker was placed in front of the specimen, driven by signals generated from a signal generator (NI USB 9263) and amplified by a power amplifier (B&K Type 2718). A tiny sound pressure probe (ER-7C, Etymotic, Grove Village, IL) was placed in the ear canal within 2 mm from the eardrum to monitor the sound pressure. The vibrating velocities of the eardrum or MGM were measured by LDV (Ploytec CLV 2534-4). When measuring the vibration of the MGM, the membrane was placed on a pars tensa perforation. A laser beam was shot on and reflected by the small tapes placed on the MGM center, and the reflected light was collected by the LDV for velocity calculation. To measure the vibration of the eardrum, the small tapes were placed on the umbo or pars tensa center. The pressure and velocity data were recorded using a four-channel data acquisition device (NI USB-9234, sampling rate 52 kHz, National Instruments, Austin, TX). An in-house MATLAB program was developed for controlling the devices and data analysis. Pure tones of varying frequencies (from 500 to 16 000 Hz, 5 points per octave) were delivered by the speaker in sequence. For each frequency, the recorded pressure and velocity data were analyzed using a fast Fourier transform (FFT).

**ABR Test:** Auditory function was objectively evaluated by the frequency-specific auditory brainstem response (ABR). The ABR test of the rats was performed with hardware and software from Tucker-Davis Technologies (TDT System III; Alachua, FL, USA). Rats were anesthetized and placed on a thermostatic heating pad to maintain body temperature at 37 °C during the recording. To identify the auditory function of each ear, the acoustic signals were delivered in a closed field via an MF1 broadband speaker (TDT). The signals were tone bursts of 1 to 32 kHz in octave step, with a 10 ms duration and a 0.5 ms rise/fall time, presented at a rate of 21.1 s<sup>-1</sup>. At each frequency, the stimulation was presented in a downward sequence from 90 to 0 dB SPL in 5 dB steps. The evoked responses were collected via three subdermal electrodes, with the recording electrodes inserted at the vertex of the head and the reference and grounding electrodes at each side of the neck behind the earlobe. The responses were amplified 20 times by a PA16 preamplifier (TDT) and filtered between 100 and 3000 Hz. The ABR threshold was defined as the lowest level at which a repeatable wave III was observed.

**Statistical Analysis:** The number of replicates (*n*) and repeated experiments are shown in the figure captions or with data. All quantitative results are presented as the mean ± standard error (s.e.m). Statistical analyses were performed using the statistical package for the social sciences (SPSS) software (ver. 23; SPSS, Inc., Chicago, IL). Statistical test methods are indicated along with the data. A difference was considered statistically significant if *p* < 0.05.

## Supporting Information

Supporting Information is available from the Wiley Online Library or from the author.

## Acknowledgements

C.Y.L., Z.Y.X., and L.Z. contributed equally to this work. The authors acknowledge the financial support from Natural Science Foundation of China (82071042, 82071160, 81901709, 81870806), International Cooperation and Exchange of the National Natural Science Foundation of China (Grant No. 81720108010), Natural Science Foundation of Shanghai (20ZR1442300) and the Australian Research Council (FL180100029).

Open access publishing facilitated by The University of Melbourne, as part of the Wiley - The University of Melbourne agreement via the Council of Australian University Librarians.

## Conflict of Interest

The authors declare no conflict of interest.

## Data Availability Statement

The data that support the findings of this study are available from the corresponding author upon reasonable request.

## Keywords

broadband frequency, eardrum perforation, graphene membranes, hearing, interfaces

Received: June 18, 2022  
Published online: August 15, 2022

- [1] D. Holmes, *Nature* **2017**, 546, S5.
- [2] J. T. Cheng, A. A. Aarnisalo, E. Harrington, M. del Socorro Hernandez-Montes, C. Furlong, S. N. Merchant, J. J. Rosowski, *Hear. Res.* **2010**, 263, 66.
- [3] a) J. T. Cheng, M. Hamade, S. N. Merchant, J. J. Rosowski, E. Harrington, C. Furlong, *J. Acoust. Soc. Am.* **2013**, 133, 918; b) J. T. Cheng, A. A. Aarnisalo, E. Harrington, M. d. S. Hernandez-Montes, C. Furlong, S. N. Merchant, J. J. Rosowski, *Hear. Res.* **2010**, 263, 66.
- [4] G. Volandri, F. Di Puccio, P. Forte, C. Carmignani, *J. Biomech.* **2011**, 44, 1219.
- [5] J. P. Fay, S. Puria, C. R. Steele, *Proc. Natl. Acad. Sci. USA* **2006**, 103, 19743.
- [6] K. N. O'Connor, M. Tam, N. H. Blevins, S. Puria, *Laryngoscope* **2008**, 118, 483.
- [7] L. Motlagh Zadeh, N. H. Silbert, K. Sternasty, W. Swanepoel, L. L. Hunter, D. R. Moore, *Proc. Natl. Acad. Sci. USA* **2019**, 116, 23753.
- [8] R. Aggarwal, S. R. Saeed, K. J. Green, *J. Laryngol. Otol.* **2006**, 120, 429.
- [9] D. Holmes, *Nature* **2017**, 546, S6.
- [10] A. Rahman, M. Hultcrantz, J. Dirckx, M. von Unge, *Otol. Neurotol.* **2007**, 28, 685.
- [11] a) M. D. Polanik, D. R. Trakimas, N. L. Black, J. T. Cheng, E. D. Kozin, A. K. Remenschneider, *Otolaryngol.–Head Neck Surg.* **2020**, 162, 914; b) D. T. Kent, D. J. Kitsko, T. Wine, D. H. Chi, *JAMA Otolaryngol. Head Neck Surg.* **2014**, 140, 106.
- [12] a) H. Seonwoo, B. Shin, K. J. Jang, M. Lee, O. S. Choo, S. B. Park, Y. C. Kim, M. J. Choi, J. Kim, P. Garg, J. H. Jang, Y. H. Choung, J. H. Chung, *Adv. Healthcare Mater.* **2019**, 8, e1801160; b) S. Anand, T. Stoppe, M. Lucena, T. Rademakers, M. Neudert, S. Danti, L. Moroni, C. Mota, *Adv. Healthcare Mater.* **2021**, 10, 2002082; c) Z. Hussain, R. Pei, *Biomed. Mater.* **2020**, 16, 032004.
- [13] a) M. A. Villar-Fernandez, J. A. Lopez-Escamez, *Audiol. Res.* **2015**, 5, 117; b) B. M. Teh, R. J. Marano, Y. Shen, P. L. Friedland, R. J. Dilley, M. D. Atlas, *Tissue Eng., Part B* **2013**, 19, 116.
- [14] S. Kanemaru, H. Umeda, Y. Kitani, T. Nakamura, S. Hirano, J. Ito, *Otol. Neurotol.* **2011**, 32, 1218.
- [15] K. N. O'Connor, H. Cai, S. Puria, *J. Acoust. Soc. Am.* **2017**, 142, 2836.
- [16] K. S. Novoselov, A. K. Geim, S. V. Morozov, D.-e. Jiang, Y. Zhang, S. V. Dubonos, I. V. Grigorieva, A. A. Firsov, *Science* **2004**, 306, 666.
- [17] Q. Zhou, J. Zheng, S. Onishi, M. F. Crommie, A. K. Zettl, *Proc. Natl. Acad. Sci. USA* **2015**, 112, 8942.
- [18] a) Y. Wei, Y. Qiao, G. Jiang, Y. Wang, F. Wang, M. Li, Y. Zhao, Y. Tian, G. Gou, S. Tan, H. Tian, Y. Yang, T. L. Ren, *ACS Nano* **2019**, 13, 8639; b) H. Tian, G.-Y. Gou, F. Wu, L.-Q. Tao, Y. Yang, T.-L. Ren, in *Graphene and Its Derivatives-Synthesis and Applications*, (Eds: I. Ahmad, F. Ezema)

- IntechOpen, London **2019**; c) W. Cardenas, R.-E. Gaskell, presented at Audio Engineering Society Convention, New York, USA October **2019**.
- [19] J. Xiao, H. Zhan, X. Wang, Z. Q. Xu, Z. Xiong, K. Zhang, G. P. Simon, J. Z. Liu, D. Li, *Nat. Nanotechnol.* **2020**, *15*, 683.
- [20] a) D. Li, M. B. Müller, S. Gilje, R. B. Kaner, G. G. Wallace, *Nat. Nanotechnol.* **2008**, *3*, 101; b) H. Chen, M. B. Müller, K. J. Gilmore, G. G. Wallace, D. Li, *Adv. Mater.* **2008**, *20*, 3557.
- [21] a) J. Kim, C. H. Kim, C. H. Park, J.-N. Seo, H. Kweon, S. W. Kang, K. G. Lee, *Wound Repair Regen.* **2010**, *18*, 132; b) B. Levin, R. Rajkhowa, S. L. Redmond, M. D. Atlas, *Expert Rev. Med. Devices* **2009**, *6*, 653.
- [22] J. H. Kim, S. J. Choi, J.-S. Park, K. T. Lim, P.-H. Choung, S. W. Kim, J. B. Lee, J. H. Chung, Y.-H. Choung, *Tissue Eng., Part A* **2009**, *16*, 225.
- [23] B. J. Allardyce, R. Rajkhowa, R. J. Dilley, Z. Xie, L. Campbell, A. Keating, M. D. Atlas, M. von Unge, X. Wang, *J. Mech. Behav. Biomed. Mater.* **2016**, *64*, 65.
- [24] a) L. Zhou, M. Feng, X. Huang, M. Duan, *Acta Oto-Laryngol.* **2017**, *137*, 679; b) J. Kim, S. W. Kim, S. Park, K. T. Lim, H. Seonwoo, Y. Kim, B. H. Hong, Y. H. Choung, J. H. Chung, *Adv. Healthcare Mater.* **2013**, *2*, 1525.
- [25] X. Yang, L. Qiu, C. Cheng, Y. Wu, Z.-F. Ma, D. Li, *Angew. Chem., Int. Ed.* **2011**, *50*, 7325.
- [26] D. Li, W. Nie, L. Chen, D. McCoul, D. Liu, X. Zhang, Y. Ji, B. Yu, C. He, *J. Biomed. Nanotechnol.* **2018**, *14*, 2003.
- [27] X. Zhang, G. Jiang, Y. Cai, S. J. Monkley, D. R. Critchley, M. P. Sheetz, *Nat. Cell Biol.* **2008**, *10*, 1062.
- [28] a) D. Xue, E. Chen, H. Zhong, W. Zhang, S. Wang, M. U. Joomun, T. Yao, Y. Tan, S. Lin, Q. Zheng, Z. Pan, *Int. J. Nanomed.* **2018**, *13*, 5799; b) J. Han, Y. S. Kim, M. Y. Lim, H. Y. Kim, S. Kong, M. Kang, Y. W. Choo, J. H. Jun, S. Ryu, H. Y. Jeong, J. Park, G. J. Jeong, J. C. Lee, G. H. Eom, Y. Ahn, B. S. Kim, *ACS Nano* **2018**, *12*, 1959.
- [29] J. Lu, C. Cheng, Y.-S. He, C. Lyu, Y. Wang, J. Yu, L. Qiu, D. Zou, D. Li, *Adv. Mater.* **2016**, *28*, 4025.
- [30] G. R. Merchant, S. N. Merchant, J. J. Rosowski, H. H. Nakajima, *Hear. Res.* **2016**, *341*, 19.
- [31] S. E. Voss, J. J. Rosowski, S. N. Merchant, W. T. Peake, *J. Acoust. Soc. Am.* **2001**, *110*, 1432.
- [32] D. Li, M. B. Muller, S. Gilje, R. B. Kaner, G. G. Wallace, *Nat. Nanotechnol.* **2008**, *3*, 101.
- [33] L. Zhou, N. Shen, M. Feng, H. Liu, M. Duan, X. Huang, *Comput. Methods Biomech. Biomed. Eng.* **2019**, *22*, 1093.
- [34] J. Zhang, J. Tian, N. Ta, Z. Rao, *J. Acoust. Soc. Am.* **2018**, *143*, 2768.